An adaptive combustion framework

By Y. C. See, H. Wu, Q. Wang AND M. Ihme

1. Motivation and objectives

Despite significant progress in combustion modeling, considerable challenges remain in high-fidelity simulations of chemical reacting flows (Pitsch 2006). One of these challenges is the high computational cost associated with the utilization of detailed chemistry kinetics in simulations of realistic combustion devices (Lu & Law 2009). Currently, most simulations of turbulent flames usually employ some variant of lower-dimensional manifold description (Pope 2012). Common to these techniques is the representation of the thermochemical state space in terms of a reduced set of scalars whose evolution is described by the solution of transport equations. Different manifold techniques for combustion applications have been developed (Pope 2012), and they can be distinguished in chemistry manifolds (Maas & Pope 1992; Lam & Goussis 1994), reaction-transport manifolds (van Oijen *et al.* 2001; Gicquel *et al.* 2000; Bykov & Maas 2007; Pierce & Moin 2004), and thermodynamic manifolds (Keck & Gillespi 1971; Ren *et al.* 2011; Hiremath *et al.* 2010).

Common to all predictive simulations of combustion devices is the issue of selecting a particular combustion model. This selection is typically guided by factors such as knowledge about the underlying combustion physics, operating conditions, quantities of interest (QoI), computational expenses, necessary model-implementation efforts, and – to some extent – also by the bias of the user. Often different models provide comparable predictions for applications that are represented by canonical flames, single combustion regimes, high Damköhler or low Karlovitz numbers, and simple gaseous fuels. However, these combustion models invoke specific assumptions and approximations, and their predictive capability reduces with increasing combustion-physical complexity. Furthermore, there are no well-established approaches to the model selection process to guarantee the accurate reproduction of relevant combustion-physical processes.

The objective of this work is to develop a novel fidelity-adaptive model (FAM) paradigm for the dynamic utilization of different manifold representations to describe chemically reacting flows. Specifically, by combining different manifold representation, FAM enables a general adaptation of combustion submodels to the underlying flow-field representation, thereby providing an accurate description of the combustion-physical complexity. The key attributes of FAM consist in (i) the user-specific selection of a set of combustion models that can be represented by a manifold (such as chemistry, mixing, or reaction-diffusion manifolds), (ii) a quantity of interest (such as temperature, carbon monoxide, nitric oxide, or other pollutants), and (iii) a cost function to describe the desirable cost and accuracy in representing the QoI. Subject to this information, a particular manifold candidate is locally selected which minimizes the cost function. As such, FAM provides direct error control and dynamically adapts the model fidelity so that regions of different combustion-physical complexity are represented by the most appropriate model formulation. Regions that are adequately represented by inert mixing, equilibrium compositions, or quasi-1D premixed and diffusion flame structures are modeled using computationally

efficient flamelet formulations, and topologically complex and multidimensional combustion processes that control flame dynamics, ignition, flame-stabilization, extinction, and blow-out are described using models at higher fidelity. The flexibility in the selection of the threshold on the cost function enables consideration of the computational cost, since the demand for model accuracy and computational expenses can vary at different stages of the design cycle. Beyond the specification of the set of manifold candidates, QoI, and threshold (error control parameter), FAM requires no additional user input. The local selection of the submodel is determined using the manifold departure function as a metric for evaluating model accuracy. Therefore, FAM can accommodate different combustion submodels without the requirement for expert knowledge on the model selection. Quantities of interest and error threshold values are usually known requirements on combustion simulations.

The proposed fidelity-adaptive model has the following main ingredients: (i) a metric for determining the proximity of the local flow-field to the combustion manifold, (ii) a procedure for assigning a combustion model locally, and (iii) a domain decomposition method to partition the flow-field domain based on the underlying combustion-physical complexity and model assignment. The first two properties are necessary to facilitate the objective assignment of combustion submodels. Since the model assignment is local, the domain decomposition capability is required to achieve optimal computational efficiency and minimize computational overhead by treating each submodel locally.

2. Governing equations and manifold models

2.1. *Governing equations*

The spatio-temporal evolution of a chemically reacting flow is described by the solution of the variable-density Navier-Stokes equations,

$$D_t\rho = -\rho\nabla\cdot\boldsymbol{u}\,, \tag{2.1a}$$

$$\rho D_t\boldsymbol{u} = -\nabla p + \nabla\cdot\left[\mu\left(\nabla\boldsymbol{u}\right) + \mu\left(\nabla\boldsymbol{u}\right)^T - \frac{2}{3}\mu\mathbf{I}\nabla\cdot\boldsymbol{u}\right]\,, \tag{2.1b}$$

where D_t represents the substantial derivative, ρ is the density, $\boldsymbol{u}$ is the velocity vector, p is the pressure, and μ is the dynamic viscosity. Conservation equations for thermochemical quantities are written in general form as

$$\rho D_t\boldsymbol{\phi} = \nabla\cdot\left(\rho\boldsymbol{\alpha}_\phi\nabla\boldsymbol{\phi}\right) + \dot{\boldsymbol{\omega}}_\phi\,, \tag{2.2}$$

where $\boldsymbol{\phi}\in\mathbf{R}^{N_\phi}$ is the thermochemical state vector, consisting of the vector of species mass fractions, $\boldsymbol{Y}$, and enthalpy; $\dot{\boldsymbol{\omega}}_\phi$ is the corresponding source term, and the vector of scalar diffusivities is denoted by $\boldsymbol{\alpha}_\phi$. Equations (2.1) and (2.2) are coupled by a state equation, which is here given in implicit form of

$$0 = f(p,\rho,\boldsymbol{\phi})\,. \tag{2.3}$$

In the present study we consider the ideal gas law, so that Eq. (2.3) reduces to $p=\rho RT$, with R being the mixture-averaged gas constant.

2.2. *Manifold methods*

Because of the large number of species required to describe the chemical conversion, it is usually unfeasible to solve the full set of N_ϕ species transport equations in Eq. (2.2).

As a remedy, manifold-type combustion models have been developed, in which the N_ϕ-dimensional state vector is represented in terms of a low-dimensional manifold, written as

$$\boldsymbol{\phi} \simeq \widehat{\boldsymbol{\phi}} = g(\boldsymbol{\psi})\,, \tag{2.4}$$

where $\widehat{\boldsymbol{\phi}} \in \mathbf{R}^{N_\phi}$ is the thermochemical state vector that is described by the manifold and $\boldsymbol{\psi} \in \mathbf{R}^{N_\psi}$ is the state vector that is used to parameterize the manifold. The spatio-temporal evolution of the manifold-describing state vector is written as

$$\rho D_t \boldsymbol{\psi} = \nabla \cdot (\rho \boldsymbol{\alpha}_\psi \nabla \boldsymbol{\psi}) + \dot{\boldsymbol{\omega}}_\psi\,. \tag{2.5}$$

The vector $\boldsymbol{\psi}$ may include a subset of species mass fractions, derived quantities such as mixture fraction or reaction progress variable, and flow-field describing quantifies such as strain rate or scalar dissipation. While different manifolds usually share the same definition for $\widehat{\boldsymbol{\phi}}$, the structure of the transported quantities $\boldsymbol{\psi}$ and the functional relation g exhibits considerable variations. For example, in the flamelet/progress variable (FPV) model, $\widehat{\boldsymbol{\phi}} = g(Z, C)$, where Z is the mixture fraction, C is the reaction progress variable and g is constructed by solving steady laminar non-premixed flamelet equations. The evolution of $\boldsymbol{\psi}$ is usually calculated explicitly, and the thermochemical information required to carry out the calculation can be obtained via the functional relation of Eq. (2.4). Therefore, by using the manifold model, the number of equations to be solved is reduced from N_ϕ to N_ψ. Since $N_\psi \ll N_\phi$, the utilization of a manifold can significantly reduce the computational cost. In the case where $N_\psi = N_\phi$, the manifold reduces to that of the complete chemical mechanism.

3. FAM framework

3.1. *Framework requirements*

As mentioned in Section 1, the FAM framework consists of three main components. The guiding principles employed in designing each of these components are discussed here.

The manifold assessment method should yield an estimation of the modeling error of unrepresented quantities described by lower-dimensional manifolds. One approach is to verify the assumptions employed in constructing the manifold. However, this requires the true solution of the configuration, which is often not available prior to simulations. Moreover, effects of violating modeling assumptions on simulations accuracy are difficult to quantify. Therefore, this manifold assessment method should only depend on manifold properties and the local flow-field of the represented variables. Direct source term evaluation also needs to be avoided due to the high computational cost associated with it.

In the model assignment step, the manifold assessment method should be utilized to determine which manifold is suitable for the corresponding local flow topology. This procedure needs to be objective and requires minimal expert knowledge. Nevertheless, user input is still needed to select a subset of unrepresented quantities from which the manifold accuracy can be assessed. Considering all unrepresented quantities may incur significant computational cost as this assessment procedure is expected to be preformed everywhere and there can be a large number of unrepresented quantities. Since the selected unrepresented quantities are usually of interest to the user, they are referred to as quantities of interest in the remainder of this paper.

The model assignment process should also consider an error control parameter with

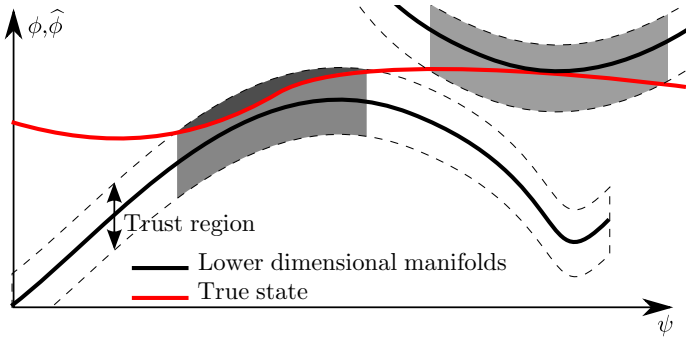

FIGURE 1. An illustration of the trust region concept.

respect to the quantities of interest. This error control parameter represents the user's preference in terms of simulation accuracy and computational efficiency. This feature allows the solver to apply more efficient lower-dimensional manifold representations when predicting robust and insensitive quantities such as major species. Simultaneously, the solver should also attempt to use more accurate higher-dimensional manifold representations when sensitive quantities such as pollutant emissions are of interest.

After the appropriate combustion model has been assigned, the solver needs to transport the corresponding set of scalars for a given combustion model in different regions of the domain. One of the solution strategies is to perform domain decomposition to create subdomains such that each will contain only one combustion model. Therefore, the set of transported scalars is the same within in each subdomain, and the numerical treatment is similar to that of employing a single combustion model. Finally, coupling strategies are deployed to determine the appropriate quantities for which matching conditions are enforced at subdomain boundaries.

3.2. *Trust region*

Based on the framework requirement outlined in Section 3.1, we introduce the concept of a manifold trust region as the core of the FAM framework. As illustrated in Figure 1, the trust region of a manifold model contains the lower-dimensional subspace and a small deviation from it. The model is considered as trustworthy and applicable if the true state is within the trust region. This decision is local in space and time. As the true state evolves in the state space, it may intersect with trust regions of different models. Accommodating this time-dependent behavior requires a dynamic model assignment procedure.

The trust region of a manifold is defined by a user-specified threshold ϵ and a measurement of the proximity $\mathcal{D}$ between $\widehat{\boldsymbol{\phi}}$ and $\boldsymbol{\phi}$ as $\{\boldsymbol{\psi} \in \mathbf{R}^{N_\psi}, \mathcal{D}(\widehat{\boldsymbol{\phi}}, \boldsymbol{\phi}) < \epsilon\}$. $\mathcal{D}$ is used to assess the manifold accuracy and a simple choice of $\mathcal{D}$ would be the Euclidean distance. However, the true state $\boldsymbol{\phi}$ is usually unknown prior to simulations so that the Euclidean distance cannot be evaluated in predictive applications. Therefore, we will develop an alternative measurement of the proximity, $\mathcal{L}_f$, which only requires a local scalar field of transported quantities $\boldsymbol{\psi}$ and the respective modeled state $\widehat{\boldsymbol{\phi}}$.

3.3. *Rate of departure from the manifold*

For a combustion manifold M, the modeled quantity $\widehat{\boldsymbol{\phi}}$ is directly evaluated using the functional relation described in Eq. 2.4. Therefore, its dynamics is implicitly governed

by

$$D_t\widehat{\boldsymbol{\phi}}_\alpha = \frac{\partial\widehat{\boldsymbol{\phi}_\alpha}}{\partial\boldsymbol{\psi}_\beta}\cdot D_t\boldsymbol{\psi}_\beta\,, \tag{3.1}$$

while the evolution of the true thermochemical state $\boldsymbol{\phi}$ is determined by the governing equation in Eq. 2.2. The difference in their formulas embeds the possible inconsistency between the dynamics of $\boldsymbol{\phi}$ and $\widehat{\boldsymbol{\phi}}$, which is the source of error for using the manifold model. In this section, we will develop a new measurement of proximity by assessing such inconsistencies. Analysis of the dynamics on manifolds has been performed previously by Pope (2012) in a different context.

To make a fair quantitative assessment of the inconsistency between $\boldsymbol{\phi}$ and $\widehat{\boldsymbol{\phi}}$, we consider how fast $\boldsymbol{\phi}$ and $\widehat{\boldsymbol{\phi}}$ will depart from each other starting from the same point by evaluating

$$D_t\boldsymbol{\Delta}|_{\boldsymbol{\Delta}=0} = D_t\boldsymbol{\phi}|_{\boldsymbol{\phi}=\widehat{\boldsymbol{\phi}}} - \frac{\partial\widehat{\boldsymbol{\phi}}}{\partial\boldsymbol{\psi}_\beta}D_t\boldsymbol{\psi}_\beta \tag{3.2}$$

$$= \frac{1}{\rho}\nabla\cdot(\rho\alpha_\phi\nabla\boldsymbol{\phi})|_{\boldsymbol{\phi}_\alpha=\widehat{\boldsymbol{\phi}}_\alpha} + \Omega^\phi_\alpha|_{\boldsymbol{\phi}_\alpha=\widehat{\boldsymbol{\phi}}_\alpha} - \frac{\partial\widehat{\boldsymbol{\phi}}_\alpha}{\partial\boldsymbol{\psi}_\beta}\frac{1}{\rho}\nabla\cdot(\rho\alpha_\beta\nabla\psi_\beta) + \dot{\omega}^\phi_\beta\,, \tag{3.3}$$

where $\boldsymbol{\Delta} = \boldsymbol{\phi} - \widehat{\boldsymbol{\phi}}$. Since Eq. 3.2 represents the initial growth rate of the manifold error, it is referred to as the rate of departure from the manifold (RDM) and is denoted by $\mathcal{R}$. The evaluation of $\mathcal{R}$ takes only the local scalar field of $\boldsymbol{\psi}$ and $\widehat{\boldsymbol{\phi}}$ as inputs. The term $D_t\boldsymbol{\psi}_\beta$ is readily computed from transporting $\boldsymbol{\psi}$ and the $\dot{\omega}^\phi_\alpha|_{\boldsymbol{\phi}_\alpha=\widehat{\boldsymbol{\phi}}_\alpha}$ is on the manifold, which means it is either pre-tabulated or can be calculated at a reduced cost.

The rate of departure from the manifold is also physically insightful in terms of interpreting the source of error for a given combustion model. Applying Eq. 3.2 to a set of flamelet models shows that the deviations from the model are initiated by the discrepancy between the true scalar dissipation rate χ with the explicitly or implicitly assumed scalar dissipation rate $\hat{\chi}$, weighted by the manifold curvature (Pope 2012). The manifold curvature is usually large at places where chemical reactions are active.

3.4. *Quantities of interest*

So far, we have developed the concept of RDM, which can be used to assess the inconsistency between the dynamics of the approximated and the true states. However, $\mathcal{R}$ as an n-dimensional quantity is not a well-defined measure and the notion of the quantities of interest is absent.

The solution is to measure the magnitude (length) of $\mathcal{R}$ projected onto the subspace that is spanned by the quantities of interest denoted by $\mathcal{Q}$. This measurement, named as loss of fidelity, can be expressed as

$$\mathcal{L}^\mu(\boldsymbol{\psi}) = \frac{1}{n(S_q)}\sum_{\alpha\in\mathcal{Q}}\left|\frac{\mathcal{R}^\mu_\alpha}{C_\alpha}\right|\,, \tag{3.4}$$

where μ denotes the combustion model, with respect to which the RDM is evaluated, and C_α is a scaling factor, which is chosen to be the reference chemical source term in this study. Since quantities excluded from $\mathcal{Q}$ are not used in evaluating Eq. 3.4, calculations of the corresponding elements of $\mathcal{R}$ can be avoided, so that with a reasonable number of quantities of interest and candidate models, the computation of $\mathcal{L}$ should incur negligible overhead.

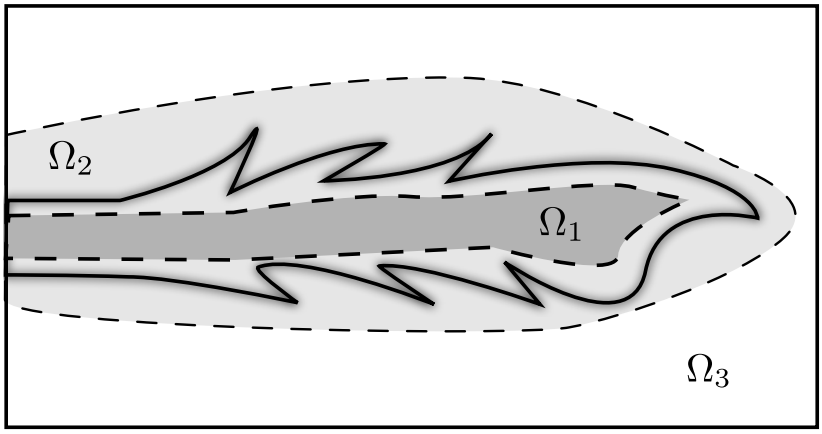

FIGURE 2. An illustration of the zonal approach in a jet flame configuration.

3.5. *Error control*

The quantity $\mathcal{L}$ is the new measure of the proximity between $\widehat{\boldsymbol{\phi}}$ and $\boldsymbol{\phi}$, which does not rely on the distance between the states but the inconsistency between their dynamics. Consequently, the new trust region is thus defined as $\{(\boldsymbol{\psi} \in \mathbf{R}^{N_\psi}, \mathcal{L}(\boldsymbol{\psi}) < \epsilon\}$, which is used to determine which manifold model to use in this adaptive framework.

The error control parameter ϵ is a user-defined quantity that regulates the trust region size. By adjusting ϵ, users can vary the overall cost of the simulation and change the usage of models at different fidelity levels. In addition, since $\mathcal{L}^\mu \equiv 0$ when μ is the detailed chemistry model, the region where no manifold model is deemed sufficiently accurate, the detailed chemistry model will be applied locally.

The decision process can also be cast as a dynamic control/optimization problem. The resulting strategy is the same as thresholding $\mathcal{L}$, which is an intuitive approach under the trust region concept.

3.6. *Domain decomposition and coupling strategies*

As developed in the previous sections, both $\mathcal{R}$ and $\mathcal{L}$ are field quantities that vary in space. Therefore, the resulting model assignment is usually spatially heterogeneous, as illustrated in Figure 2.

Based on the local model assignment procedure, the full computational domain Ω is decomposed into p connected and non-overlapping subdomains Ω_i such that

$$\Omega_i \cap \Omega_j = \emptyset \quad \forall i\,, j \quad \text{and} \quad i \neq j\,, \tag{3.5}$$

$$\cup \Omega_i = \Omega. \tag{3.6}$$

The assigned combustion model is homogeneous within each subdomain Ω_i, but it is distinct from the models used in its adjacent domains. In the most general settings, other physics submodels and discretizations can be utilized adaptively and vary across subdomains (Almgren *et al.* 1998).

The subdomains need to be coupled in simulations, and there are several approaches to conciliate a pair of chemical manifolds at subdomain interfaces. These approaches can mostly be categorized into weak and strong coupling strategies. These two strategies are differentiated by the set of quantities for which the continuity is enforced. In the weak coupling strategy, only the continuity of represented quantities is enforced at the

subdomain interfaces, i.e.

$$\boldsymbol{\psi}_i(\mathbf{x}) = \boldsymbol{\psi}_j(\mathbf{x}) \quad \forall \mathbf{x} \in \Omega_i \cap \Omega_j. \tag{3.7}$$

This coupling approach is simple to evaluate, but the sets of represented quantities for two manifolds under consideration must be the same. In addition, this approach may lead to discontinuities for the unrepresented variables at the interfaces as the chemical manifolds can be different even for the same values of ψ.

The strong coupling method has a more stringent requirement that the thermo-chemical state variables must be continuous across subdomains. This approach enforces that

$$\widehat{\boldsymbol{\phi}}_i(\mathbf{x}) = \widehat{\boldsymbol{\phi}}_j(\mathbf{x}) \quad \forall \mathbf{x} \in \Omega_i \cap \Omega_j. \tag{3.8}$$

With this constraint, the continuity of the unrepresented variables is guaranteed but the unrepresented quantities may not be smooth across subdomain interfaces. Furthermore, it may not be possible to find a combination of unrepresented quantities that can satisfy Eq. 3.8 as the manifolds of two subdomains may be incompatible.

Since the two coupling approaches have different desirable properties, we utilize both types of coupling strategies in this work. Depending on the pair of manifolds under consideration, one coupling strategy may be more suitable. In the current work, the strong coupling is enforced at the interfaces where lower-dimensional manifolds are interacting with the complete chemistry kinetics. Strong coupling is the natural choice in this scenario as there are no unrepresented quantities in the complete model. At interfaces where both models are of lower-dimensional manifolds, only weak coupling is enforced. As mentioned earlier, strong coupling may not always be possible for this type of interface. Since the rate of departure from the manifold, $\mathcal{R}$, is capable of detecting the discontinuity which may rise from such treatment, interfaces between two lower-dimensional manifolds are expected to be limited so the weak coupling should be utilized rarely in this framework.

4. Model problem: tribrachial flame

To demonstrate the FAM framework, we consider a tribrachial flame configuration (Chung 2007). This flame configuration contains different combustion regimes, introducing substantial challenges to the the accuracy of most single-regime combustion models. Generally, tribrachial flames are usually present in flows with a stratification of reactants. This flame, shown in Figure 3, consists of lean and rich premixed flame branches, and a diffusion flame in between the two premixed branches. Within the diffusion flame, excess fuel from the rich premixed flame branch reacts with the excess oxidizer from the lean premixed branch (Echekki & Chen 1998). The three flame branches meet at the triple point of nearly stoichiometric composition. Furthermore, the mixture in the diffusion branch is usually close to chemical equilibrium, and the diffusion flame is less prominent than the two premixed flames (Oijen & de Goey 2006).

Numerical models have been developed and utilized in the tribrachial flame configuration. Oijen & de Goey (2006) studied the relationship between flame propagation and levels of stratification using the flamelet-generated manifold (FGM) model. In their study, a two-dimensional manifold with progress variable and mixture fraction as the controlling variables were used. The structure and behavior of flamelets in both premixed and diffusion flame branches were reproduced reasonably. As an extension to the flamelet approach, Knudsen & Pitsch (2011) proposed a mixed-regime flamelet model and compared the results with detailed simulations using finite rate chemistry. A new

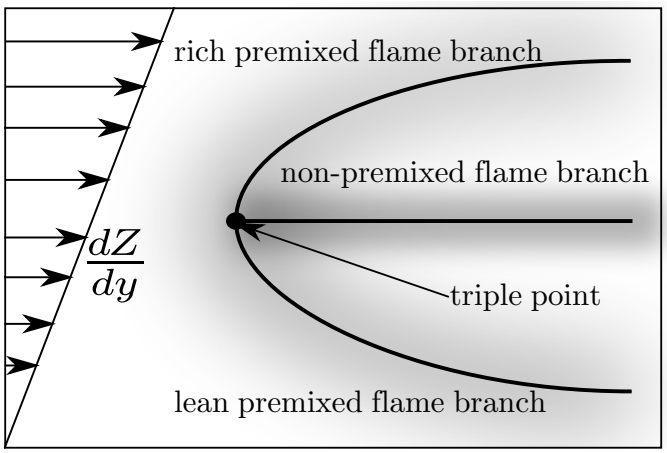

FIGURE 3. A schematic of the flame structure for a tribrachial flame.

regime indicator has been developed to allow the application of the premixed and the non-premixed flamelet model simultaneously.

4.1. *Computational setup*

The tribrachial flame configuration that is under consideration is a 2D laminar methane-air flame. The level of stratification is quantified in terms of the mixture-fraction gradient in the transverse direction dZ/dy. Using the specified value of dZ/dy, a linear profile of mixture fraction with the corresponding slope is prescribed at the inflow. Furthermore, the stoichiometric value of the profile is enforced to be centered in the computational domain and the profile is also bounded by the realizable limit values of mixture fraction. At the inlet boundary, the mixture is assumed to be unreacted so that the species composition can be described by the mixture fraction alone. The inlet velocity profile is prescribed by a plug flow.

Throughout this work, we specify $dZ/dy = 1/L$ with $L = 0.02$ m, $T = 300$ K and $p = 1$ bar in all simulations. The computational domain is $(0.75 \times 1)L^2$ in the transverse and streamwise directions, respectively. At the prescribed level of stratification, the tribrachial flame envelope occupies a significant area in the domain. At the same time, the flame envelope also has sufficient clearance from the lateral no-slip wall boundaries to avoid flame-wall interaction.

A variable density low-Mach number solver is utilized for the tribrachial flame simulations The temporal discretization for this solver is a two-stage predictor-corrector scheme with a pressure Poisson corrector step. Detailed chemistry is solved using a Strang splitting scheme. Although the tribrachial flame is laminar, the flame is required to be stabilized at the same location for model comparison. Therefore, a proportional-integral-derivative (PID) controller (Bell *et al.* 2006) is utilized at the inlet to adjust the inlet axial velocity so that the flame is stabilized at the same location.

The mesh for all computations of this tribrachial flame configuration uses 800×600 grid points with uniform mesh size. The element length for this mesh is $20\mu m$, corresponding to approximately 20 grid points across a planar stoichiometric methane-air premixed flame at the $T = 300$K and $p = 1$bar. Although the configuration is steady, the simulation is unsteady in nature and the time-step size is $5\mu s$. The GRI 3.0 chemical mechanism (Smith *et al.* 2000) is used in all combustion submodels that are considered in

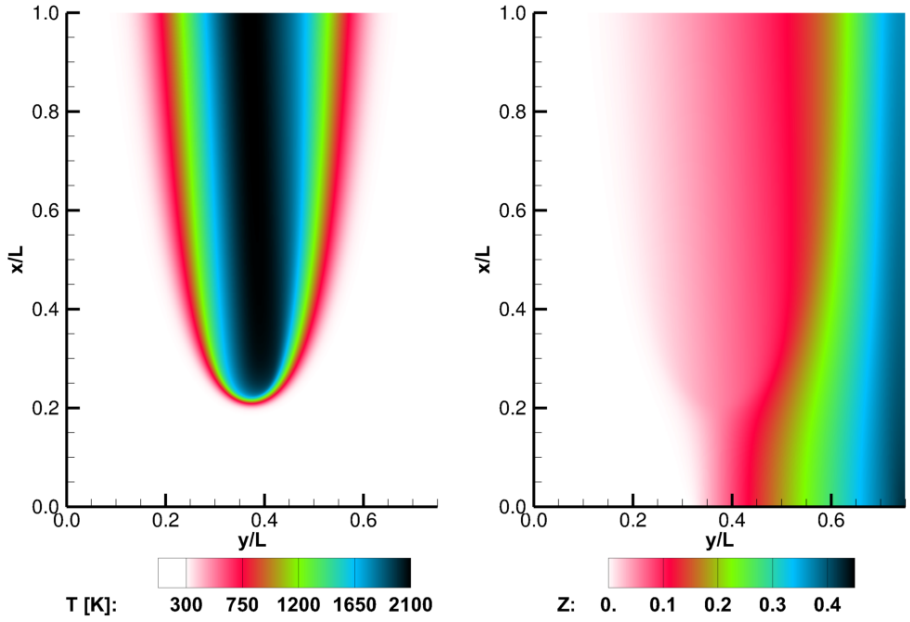

(a) Temperature field. (b) Mixture fraction field.

FIGURE 4. Results of detailed chemistry simulation of the tribrachial flame configuration.

this work. Unity Lewis number also is assumed in all simulations. In addition to a detailed chemistry model for the general description of flame topologies, the lower-dimensional manifolds that are considered here are the flamelet progress variable approach (FPV) by Pierce & Moin (2004) for diffusion flames, flamelet prolongation of ILDM (FPI) by Gicquel *et al.* (2000) for premixed flames and the inert mixing manifold. For the FPV and FPI models, the progress variable is defined to be $C = Y_{\mathrm{CO}} + Y_{\mathrm{CO_2}} + Y_{\mathrm{H_2}} + Y_{\mathrm{H_2O}}$.

To obtain a reference solution to assess the performance of the FAM-formulation, a simulation with detailed chemical kinetics model is performed. Results from this simulation are shown in Figure 4. From the temperature field, it is clear that the maximum temperature is found along the centerline where the mixture is near stoichiometric condition. Furthermore, the temperature field also indicates that the flame is anchored at $x/L = 0.25$, showing that the PID-controller is able to stabilize the flame at a specified location. The inlet velocity, U_0, needed to stabilize the flame is 59.1cm/s and is in good agreement with theoretical predictions (Chung 2007). Moreover, the stabilized flame remains in the same location even after the controller has been deactivated. With this inlet velocity, the Reynolds number based on L and properties of air is approximately 800. At this condition, the flow is expected to be laminar since the heat release from combustion can further delay the transition.

5. Results

5.1. *Baseline case*

As a baseline demonstration of the FAM-formulation, the model is applied to the tribrachial flame configuration discussed in Section 4. In this case, the combustion model candidates that are considered here are (i) the inert mixing model, (ii) FPI, (iii) FPV,

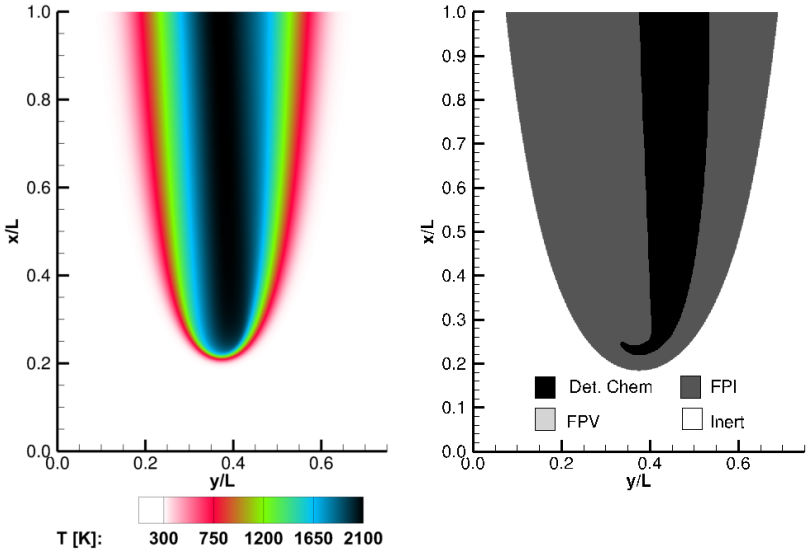

FIGURE 5. (a) Temperature and (b) model assignment field of FAM simulation at $\epsilon = 0.2$.

and (iv) the detailed chemistry description. The quantities of interest are set to be $\mathcal{Q} = \{CO_2, CO, H_2O, H_2, NO\}$. As described in Section 3.2, the trust region concept utilized in the model requires a user-selected threshold ϵ which is set to a numerical value of 0.25.

The results from the simulation obtained with FAM are shown in Figure 5. Qualitatively, the model is able to predict the general characterization of the tribrachial flame. The corresponding model assignment (Figure 5b) shows that different combustion models are utilized in this simulation. The coupling strategy discussed in Section 3.6, is able to produce a continuous temperature field without discontinuity at the subdomain interfaces. Interestingly, it can be seen from the model assignment field that the premixed model is utilized along the centerline of the flame where a non-premixed flame branch is expected, as shown in Figure 3.

To examine why the premixed model is selected over the non-premixed model near the centerline, we compare profiles of CO and NO along centerline and transverse directions in Figure 6. The results from the detailed chemistry solution are included as a reference. This comparison shows that the application of the premixed model yields predictions that are in better agreement with the reference solution than that from the non-premixed model.

5.2. *Dynamic model assignment*

Although the baseline demonstration of the FAM-formulation is a steady configuration, the model itself is constructed for unsteady applications. The model assignment field, shown in Figure 5b, is obtained after five flow-through times from an initialization with the FPI solution. It may be faster to evaluate RDM on the reference solution to obtain the final model assignment instantaneously. However, the reference solution is usually not available in most turbulent flames of interest. Therefore, it is more natural for fidelity-

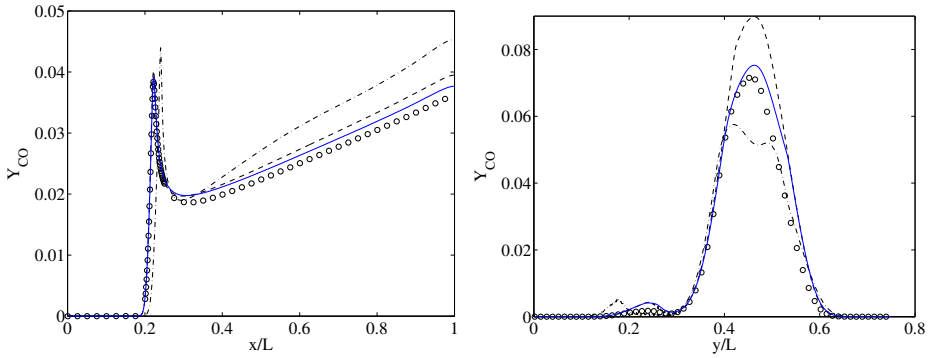

FIGURE 6. Comparison of the profiles of Y_{CO} at $y/L = 0.375$ and $x/L = 0.75$ between detailed chemistry (black open circle), FAM (blue solid line), FPV (black dashed line), and FPI (black dot-dashed line) simulations.

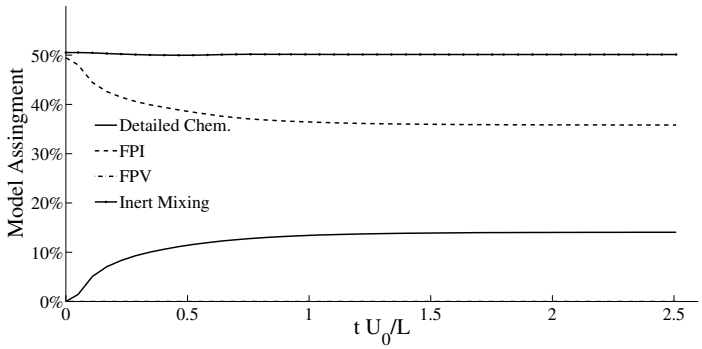

FIGURE 7. Temporal evolution of the model assignment breakdown.

adaptive simulations to be initialized from predictions that can be easily obtained with lower-dimensional manifold models.

Without initialization from a reference solution, the RDM can evolve in time as the certain regions of the simulation can become more accurate over time. To quantify the relaxation time, the time history of the model selection is illustrated in Figure 7. Initially, only the inert mixing model and the FPI model are utilized in the simulation. After a sufficient number of time-steps, the detailed chemistry region starts to emerge in the leading edge of the tribrachial flame. At around one convective time scale, the model assignment field is mostly converged. This rate of convergence is expected as abrupt changes in the flow-field can take approximately a convective time scale to fully propagate throughout the simulation domain.

In the final model assignment, the inert mixing model covers approximately half of the domain where the chemical reaction is inactive, and the detailed chemistry model covers the entire flame tip and most of the rich region. In the remaining lean and stoichiometric regions of the flame, the premixed model is utilized as it is deemed sufficiently accurate under the defined threshold.

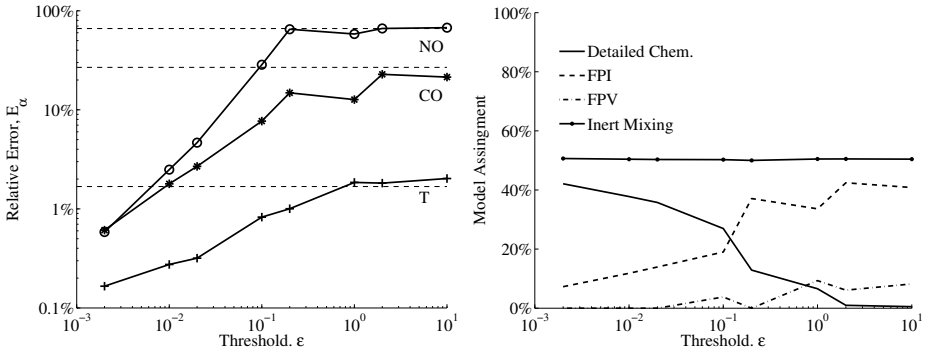

FIGURE 8. (a) Relative error of species mass fractions and (b) model assignment for the cases using $\mathcal{Q} = \{CO_2, CO, H_2O, H_2, NO\}$ at various ϵ. Dash lines are the reference FPI results, of which ϵ is not defined.

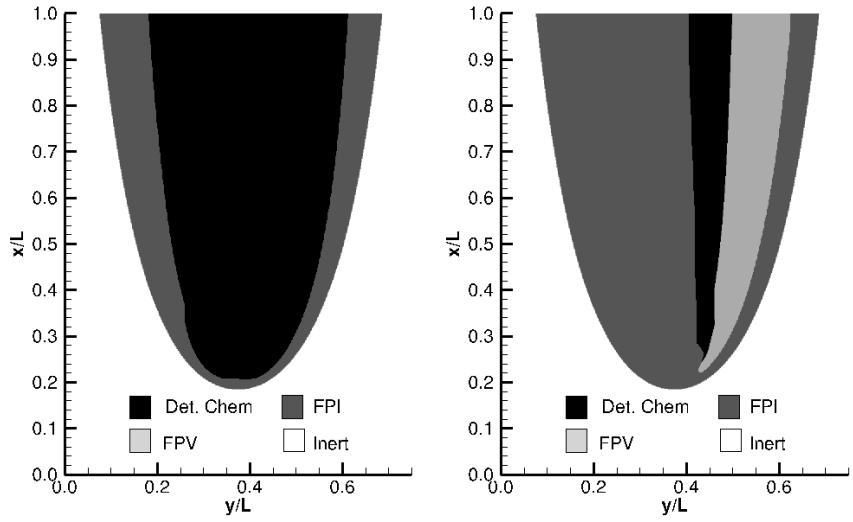

(a) $\epsilon = 2 \times 10^{-3}$ (b) $\epsilon = 1$

FIGURE 9. Model assignment for (a) $\epsilon = 2 \times 10^{-3}$ and (b) $\epsilon = 1$.

5.3. *Error control and fidelity/efficiency trade-off*

In this section, we examine the response of FAM results to different threshold levels. The set of candidate models and the set of quantities of interest are the same as the baseline case. The threshold ϵ ranges from 0.01 to 50.

The relative error E_i for $\mathcal{Q}$ as a function of ϵ is plotted in Figure 8a. E_i is defined as the $l1$-norm of the point-wise relative difference between the FAM simulation results and the detailed chemistry results. As expected, the relative error monotonically increases with increasing threshold until a plateau is reached. Even for the maximum threshold of $\epsilon = 50$, the FAM simulation results are comparable to the FPI results. As shown in

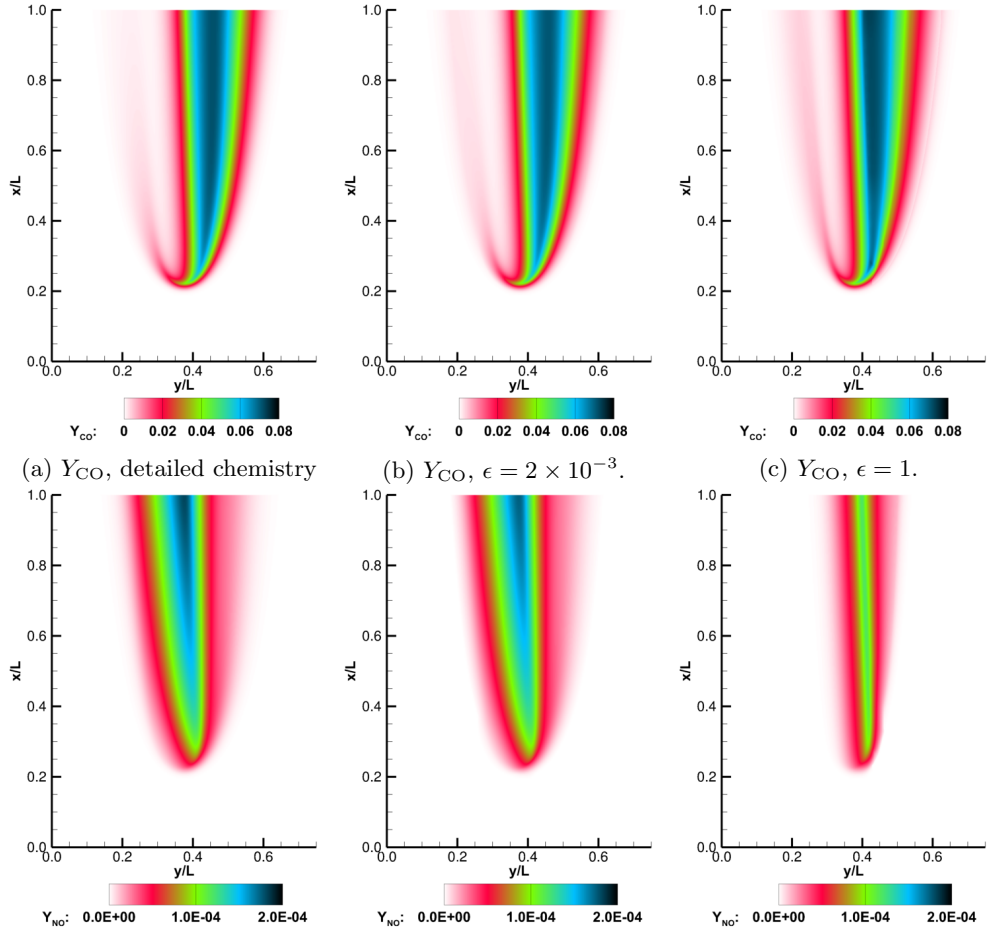

(a) Y_{CO}, detailed chemistry (b) Y_{CO}, $\epsilon = 2 \times 10^{-3}$. (c) Y_{CO}, $\epsilon = 1$.

(d) Y_{NO}, detailed chemistry (e) Y_{NO}, $\epsilon = 2 \times 10^{-3}$. (f) Y_{NO}, $\epsilon = 1$.

FIGURE 10. Y_{CO}, and Y_{NO} for detailed simulation (rightmost column), $\epsilon = 2 \times 10^{-3}$ (middle column) and $\epsilon = 1$ (leftmost column).

Figure 8a, the accuracy of different species is not uniform and the spread increases with larger threshold. For example, the error in the predicted temperature is always below 1%, while the error in Y_{NO} varies by more than two orders of magnitude.

The difficulty in predicting certain quantities accurately is illustrated in Figure 10 where the predicted NO field only begins to show reasonable agreement with the reference solution at $\epsilon = 2 \times 10^{-3}$. Compared to the higher threshold value of $\epsilon = 1$, the predicted NO profile is more consistent with the detailed chemistry simulation. As shown in Figure 9, the lower threshold simulation utilizes the detailed chemistry kinetics in most of the flame region. In comparison, the detailed chemistry region occupies only a relatively small area in the fuel-rich portion of the flame when a higher threshold is used.

Figure 8b shows the coverage of each candidate models as a function of ϵ. As expected, the adaptive model assignment shifts toward flamelet models with increasing ϵ. The usage of the detailed chemistry model drops from 40% to zero while the usage of the FPI model

increases from less than 10% to 40%. Since the configuration is designed such that the flame occupies only half of the domain, the inert mixing model consistently shows usage of 50%. The usage of the FPV model never exceeds 10%, suggesting that this model may not be suitable for this configuration.

6. Conclusions

In this paper, a fidelity-adaptive modeling framework has been developed for simulations of chemically reacting flows. This framework utilizes a domain decomposition approach in which different combustion models are assigned to each subdomain. The model assignment and subdomain partitioning are determined from a user-specified error threshold on a quantity of interest. The newly developed methodology is applied to a tribrachial flame configuration which has a non-trivial flame topology. Even at a moderate threshold value, this simulation approach utilizes a detailed chemistry description in regions where the lower-dimension manifold prediction of the quantity of interest suffers. This yields a significantly more accurate flame prediction, and the results improve with reducing error tolerance. This fidelity-adaptive modeling framework will be further extended for application to turbulent flames.

REFERENCES

Almgren, A. S., Bell, J. B., Colella, P., Howell, L. H. & Welcome, M. L. 1998 A conservative adaptive projection method for the variable density incompressible Navier-Stokes equations. *J. Comp. Phys.* **142**, 1–46.

Bell, J., Day, M., Grcar, J. & Lijewski, M. 2006 Active control for statistically stationary turbulent premixed flame simulations. *Comm. Appl. Math. Comp. Sci.* **1**, 29–51.

Bykov, V. & Maas, U. 2007 The extension of the ILDM concept to reaction-diffusion manifolds. *Combust. Theory Modelling* **11**, 839–862.

Chung, S. H. 2007 Stabilization, propagation and instability of tribrachial triple flames. *Proc. Combust. Inst.* **31**, 877–892.

Echekki, T. & Chen, J. H. 1998 Structure and propagation of methanol-air triple flames. *Combust. Flame* **114**, 231–245.

Gicquel, O., Darabiha, N. & Thevenin, D. 2000 Laminar premixed hydrogen/air counterflow flame simulations using flame prolongation of ILDM with differential diffusion. *Proc. Combust. Inst.* **28**, 1901–1908.

Hiremath, V., Ren, Z. & Pope, S. B. 2010 A greedy algorithm for species selection in dimension reduction of combustion chemistry. *Combust. Theory Modelling* **14**, 619–652.

Keck, J. & Gillespi, D. 1971 Rate-controlled partial-equilibrium method for treating reacting gas-mixtures. *Combust. Flame* **17**, 237–241.

Knudsen, E. & Pitsch, H. 2011 Capabilities and limitations of multi-regime flamelet combustion models. *Combust. Flame* **159**, 242–264.

Lam, S. H. & Goussis, D. A. 1994 The CSP method for simplifying kinetics. *Int. J. Chem. Kinet.* **26**, 461–486.

Lu, T. & Law, C. K. 2009 Toward accommodating realistic fuel chemistry in large-scale computations. *Prog. Energy Combust. Sci.* **35**, 192–215.

Maas, U. & Pope, S. B. 1992 Simplifying chemical kinetics: Intrinsic low-dimensional manifolds in composition space. *Combust. Flame* **88**, 239–264.

Oijen, J. & de Goey, L. P. H. 2006 A numerical study of confined triple flames using a flamelet-generated manifold. *Combust. Theor. Model.* **8**, 141–163.

van Oijen, J. A., Lammers, F. A. & de Goey, L. P. H. 2001 Modeling of complex premixed burner systems by using flamelet-generated manifolds. *Combust. Flame* **127**, 2124–2134.

Pierce, C. D. & Moin, P. 2004 Progress-variable approach for large-eddy simulation of non-premixed turbulent combustion. *J. Fluid Mech.* **504**, 73–97.

Pitsch, H. 2006 Large-eddy simulation of turbulent combustion. *Annu. Rev. Fluid Mech.* **38**, 453–482.

Pope, S. B. 2012 Small scales, many species and the manifold challenges of turbulent combustion. *Proc. Combust. Inst.* **34**, 1–31.

Ren, Z., Goldin, G. M., Hiremath, V. & Pope, S. B. 2011 Reduced description of reactive flows with tabulation of chemistry. *Combust. Theory Modelling* **15**, 827–848.

Smith, G. P., Golden, D. M., Frenklach, M., Moriarty, N. W., Eiteneer, B., Goldenberg, M., Bowman, C. T., Hanson, R. K., Song, S., Gardiner, Jr., W. C., Lissianski, V. V. & Qin, Z. 2000 GRI-Mech 3.0. Available from `http://www.me.berkeley.edu/gri-mech/`.